Journal of Structural Geology 32 (2010) 1792–1805

Contents lists available at ScienceDirect

Journal of Structural Geology

journal homepage: www.elsevier.com/locate/jsg

Relationship between fault growth mechanism and permeability variations with depth of siliceous mudstones in northern Hokkaido, Japan

Eiichi Ishii [a,*], Hironori Funaki [a], Tetsuya Tokiwa [a], Kunio Ota [b]

[a] Horonobe Underground Research Unit, Japan Atomic Energy Agency, Hokushin 432-2, Horonobe-cho, Hokkaido 098-3224, Japan
[b] Geological Isolation Research and Development Directorate, Japan Atomic Energy Agency, Muramatsu 4-33, Tokai-mura, Ibaraki 319-1144, Japan

ARTICLE INFO

Article history:
Received 26 January 2009
Received in revised form
6 October 2009
Accepted 30 October 2009
Available online 11 November 2009

Keywords:
Fault
Shear
Tensile
Stress
Permeability
Siliceous mudstone

ABSTRACT

In order to assess the influence of remote mean stress correlated with depth of burial on the principal mode of failure at fault tips during fault slip in a lithologically homogeneous, fractured rock mass, the growth mechanisms of strike-slip faults have been studied at outcrop-scale in the siliceous mudstones of northern Hokkaido, Japan. We take a multifaceted approach combining i) geological characterization of fractures by fracture mapping in outcrop and fracture logging of boreholes (drilling depth: $\leq$1020 m), ii) rock mechanical characterization by laboratory tests on core samples, and iii) theoretical analyses using the Griffith–Coulomb criterion. These suggested that the principal mode of failure in the mudstones is dependent, not only on rock strength, but also on remote mean stresses. During and/or after uplift and erosion the faults grew mainly by linking with adjacent faults via numerous splay cracks, formed by tensile failure above roughly 400 m depth. In contrast, below this depth, the faults grew predominantly by shear failure. Such growth mechanisms are consistent with the fact that hydraulic tests performed in boreholes show that highly permeable sections (hydraulic transmissivity: $>10^{-5}$ m^2/s) are restricted to depths of less than 400 m.

1. Introduction

Decreasing permeability with depth in fractured rock masses (e.g., at depths of less than 1 km), which is consistent with closure of pore apertures with increasing pressure (e.g., Wei et al., 1995; Öhman et al., 2005), has been widely recognized in deep drilling programs worldwide (e.g., Rhén et al., 2006; Andersson et al., 2007; Nordqvist et al., 2008). However, clear exceptions to this trend exist and numerous authors have suggested that permeability distributions in fractured rock masses are fundamentally dependent on mechanisms of their brittle deformation (e.g., Caine et al., 1996; Mazurek et al., 1996, 1998, 2003; Evans et al., 1997; Gutmanis et al., 1998; Mazurek, 1998, 2000; Bossart et al., 2001).

Sheared-joint-based faulting associated with the numerous tensile splay cracks that propagate from the tip of faults when faults slip is a well known mechanism of brittle deformation (e.g., Segall and Pollard, 1983; Martel and Pollard, 1989; Flodin and Aydin, 2004; Myers and Aydin, 2004). This style of faulting is known to significantly increase the permeability of a fractured rock mass (e.g., Mazurek et al., 1998, 2003; Dholakia et al., 1998; d'Alessio and Martel, 2004; Lunn et al., 2008; Eichhubl et al., 2009). Mazurek et al. (1998) showed that the transmissivity of groundwater inflow points in boreholes penetrating the highly consolidated and fractured marls in the central Swiss Alps decreases with depth, and indicated that the tensile splay cracks forming the fault linkages may be the actual inflow points. This is an example of an earlier study that implied a relationship between splays and permeability variations with depth. However, the relationship has not been examined in detail.

In order for tensile splay cracks to form, tensile failure is required near fault tips when fault slip occurs. However, such tensile failure may not necessarily occur under all stress states; it is possible that shear failure could occur. The principal mode of failure is also known to depend on lithology, i.e., tensile failure tends to occur in stronger rocks while shear failure tends to occur in weaker rocks (e.g., Gross, 1995; Eichhubl and Boles, 2000; Welch et al., 2009). Also concerning the principal mode of failure near fault tips during sheared-joint-based faulting, the control of failure mode by lithology is shown by field observations on the Monterey Formation of California (Dholakia et al., 1998). However, it is indicated by numerical simulations using the Griffith–Coulomb criterion that the principal mode of failure near fault tips due to fault slip depends not only on lithology but also on remote mean stress at the time of fault slip (Bourne and Willemse, 2001),

* Corresponding author. Fax: +81 1632 5 2344.
E-mail address: ishii.eiichi@jaea.go.jp (E. Ishii).

0191-8141/$ – see front matter © 2009 Elsevier Ltd. All rights reserved.
doi:10.1016/j.jsg.2009.10.012

which suggests that tensile failure tends to occur under lower remote mean stress and shear failure tends to occur under higher remote mean stress. Therefore, remote mean stress is also an important factor in failure mode, and, considering that remote mean stress is generally correlated with burial depth (e.g., Twiss and Moores, 2007), the difference in the principal failure mode with increasing burial depth may also have a direct relationship to variations in permeability with depth, as observed in fractured rock masses.

In the Horonobe area, northern Hokkaido, Japan, folded Neogene siliceous mudstone, the Wakkanai Formation (Figs. 1 and 2), is massive and lithologically homogeneous (Iijima and Tada, 1981) with very weakly developed bedding planes (Ishii et al., 2006). Faults crosscutting bedding planes at a high angle (FCBs) and bedding faults parallel to bedding are observed at outcrop-scale (Ishii and Fukushima, 2006). The FCBs are mainly strike-slip faults oblique to fold axes. Geological and hydrogeological data indicate that some of the FCBs are the main flow paths (Ishii and Fukushima, 2006; Kurikami et al., 2008; Funaki et al., 2009). Furthermore, hydraulic packer tests performed in twelve deep, vertical boreholes (drilling depth: ≤1020 m) show that the sections with highest permeability (hydraulic transmissivity: $>10^{-5}$ m^2/s) are restricted to depths of less than about 400 m in the formation (Fig. 3).

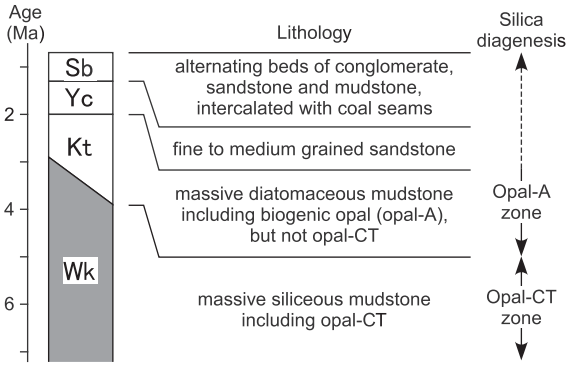

Fig. 2. Schematic columnar section in the study area (modified Ota et al., 2007). Sb: Sarabetsu Formation; Yc: Yuchi Formation; Kt; Koetoi Formation; Wk: Wakkanai Formation.

In this study, a case study addressing the influence of remote mean stress (i.e. burial depth) on the principal mode of failure

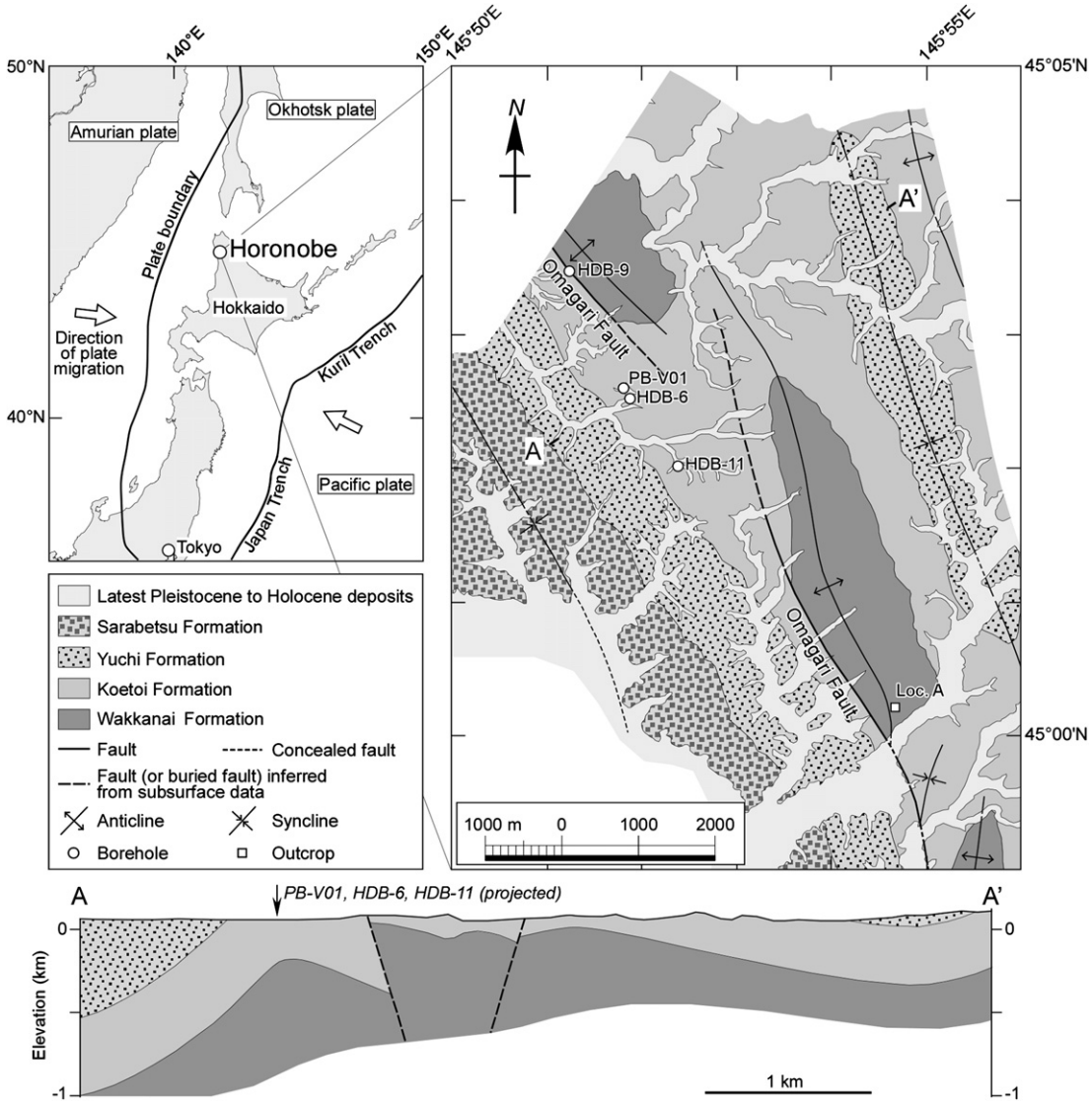

Fig. 1. Geological map and geological cross-section in the Horonobe area (after Ishii et al., 2008), showing locations of the cleared outcrop and the boreholes. Plate boundaries and directions of plate migration in location map of the left upper are from Wei and Seno (1998).

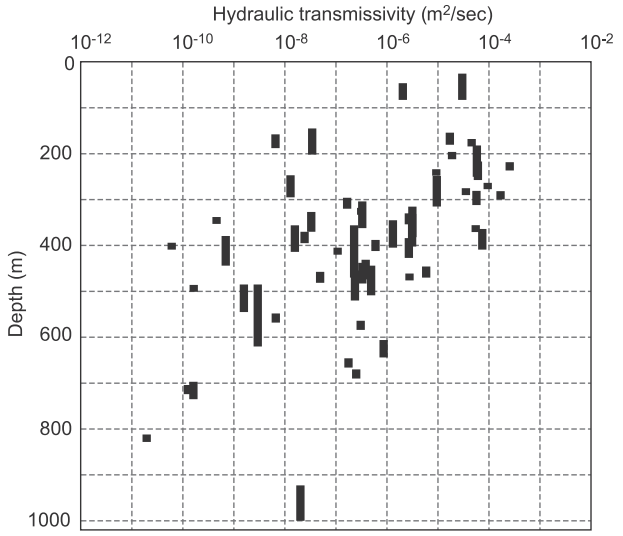

Fig. 3. Permeability of the Wakkanai Formation obtained by hydraulic packer tests in twelve vertical boreholes (HDB-1 to HDB-11 and PB-V01). Data are from Kurikami (2007) and Yabuuchi et al. (2008). Compared to the hydraulic transmissivity of similar depths, higher permeability sections tend to correspond to fractured sections. The difference in hydraulic transmissivity between a fractured section and an intact section at similar depths may be five orders of magnitude.

near fault tips during fault slip in a lithologically homogeneous, fractured rock mass is discussed. Taking it one step further, the relationship between failure mode and permeability, that is, the relationship between the growth mechanisms of the FCBs and the permeability variations with depth of the Wakkanai Formation is discussed. For this study, related to the parameter burial depth, vertical borehole data are important. However, information on the faults reliant solely on restricted information from borehole core data is not enough. Hence, a multifaceted approach combining outcrop surveying, borehole investigations, and theoretical analyses is applied for the Wakkanai Formation. The study combines i) geological characterization of fractures by fracture mapping in outcrop and fracture logging of boreholes, ii) rock mechanical characterization by laboratory tests on core samples for tensile strength and angle of internal friction, and iii) theoretical analyses using the Griffith–Coulomb criterion.

2. Geological setting

The Horonobe area is located on the eastern margin of a Neogene to Quaternary sedimentary basin located on the western side of northern Hokkaido, in a Quaternary, active foreland fold-and-thrust belt near the boundary between the Okhotsk and Amurian plates (e.g., Yamamoto, 1979; Wei and Seno, 1998; Ikeda, 2002; Fig. 1). The basin grades upward stratigraphically from the Wakkanai Formation (massive siliceous mudstones including opal-CT), to the Koetoi Formation (massive diatomaceous mudstones including opal-A, but not opal-CT), to the Yuchi Formation (fine to medium grained sandstones), and lastly to the Sarabetsu Formation (alternating beds of conglomerate, sandstone and mudstone, intercalated with coal seams), overlain by late Pleistocene to Holocene deposits (Figs. 1 and 2). The Wakkanai and Koetoi Formations have the following characteristics: i) they have fairly uniform muddy facies with rare intercalation of pyroclastic sediments (Mitsui and Taguchi, 1977; Tada and Iijima, 1982; Ishii et al., 2008), ii) bedding planes are difficult to recognize due to their homogeneity, though planes can be recognized, albeit weakly by electrical micro-imaging (Ishii et al., 2006), iii) they are non-calcareous, diatomaceous siliceous rocks but relatively argillaceous (Iijima and Tada, 1981; Tada and Iijima, 1982) and have Al_2O_3 content of 8–11% (Ishii et al., 2007; Hiraga and Ishii, 2008), iv) mineral compositions consist of silica minerals (opal-A and/or opal-CT) and small amounts of quartz, feldspar, clay minerals (kaolinite, smectite, illite and/or chlorite), pyrite, and carbonates (siderite and/or magnesite) (Ishii et al., 2007), and v) they resemble siliceous shale units of the Monterey Formation of California (e.g., Murata and Nakata, 1974; Isaacs, 1982) in rock type. This study focused on the siliceous mudstone composing the Wakkanai Formation, which was formed by induration of the diatomaceous mudstone composing the Koetoi Formation during progressive burial diagenesis of silica minerals, i.e., conversion of opal-A to opal-CT (Fukusawa, 1985). Furthermore, stiff siliceous mudstones, termed opaline chert, are observed in the upper part of the Wakkanai Formation at the surface (Fukusawa, 1985). It was suggested by Iijima and Tada (1981) that the opaline cherts formed in the upper part of the opal-CT zone (near the opal-A zone) by additional silica cementation during uplift of the Neogene noncalcareous siliceous rocks in northern Japan. The opaline cherts are inter-layered with siliceous mudstones in the upper part of the Wakkanai Formation at the surface (e.g., Fig. 4), whereas, in core samples, such opaline

Fig. 4. Photograph of the horizontal bedrock exposure made by stripping with heavy equipment (modified Ishii and Fukushima, 2006). The opaline chert layer parallel to bedding plane (strike/dip: N10°W/30°E) is displaced by the major FCBs (strike/dip: N40°–56°W/54°–90° N) in the center of the outcrop.

cherts are rarely observed and the harder siliceous mudstones are common in the upper part of the Wakkanai Formation.

In the center of the Horonobe area, a map-scale fault, the Omagari Fault, strikes NNW–SSE, generally subparallel to major folds developed in the area. The Omagari Fault is an oblique fault with reverse dip-slip and sinistral strike-slip components, which exhibits an east–west step-over at surface that possibly converges in the subsurface (Ishii et al., 2006). A previous study on burial diagenesis in this area indicates that the Wakkanai Formation was buried to at least a depth of 1 km. Flexural folding of the sediments began between 2.2 and 1.0 Ma. The study area was exposed at approximately 1.0 Ma, at the latest (Ishii et al., 2008).

3. Methodology

3.1. Geological characterization of fractures

Fracture mapping of an exposure of the Wakkanai Formation bedrock (Loc. A in Fig. 1) and fracture logging of four boreholes (HDB-6, HDB-9, HDB-11 and PB-V01; Fig. 1) were carried out for the geological characterization of fractures. Fracture mapping of horizontal exposures of bedrock is considered important for geometrical analysis of strike-slip faults such as the FCBs. However, because there are few bedrock exposures in this area due to the abundance of vegetation and overburden, a horizontal exposure, 32.5 m × 25.5 m (Fig. 4), was cleared with heavy equipment for fracture mapping (Ishii and Fukushima, 2006). Data on the following fracture characteristics were collected: fracture orientations, lengths, widths and termination styles, filling materials, failure modes, sense of displacement, and crosscutting relationships. Stress directions for displacement along the oblique faults were determined by the multiple inverse method of Yamaji (2000). In the borehole investigations, the following data on natural fractures in the core were collected: depth of intersections, frequencies, fracture orientations and widths, filling materials, failure modes, and sense of displacement. Fractures induced by drilling or handling were excluded following criteria established by Kulander et al. (1990). Fracture orientations were also determined by detailed correlation between the core data and the acoustic imagery data obtained by the borehole televiewer survey (BHTV). Concerning BHTV, even if a borehole wall is composed of dark-colored rock such as siliceous mudstone and/or is coated with drilling mud, or even if a borehole is filled by cloudy borehole water, BHTV can provide useful images of the borehole wall (Williams and Johnson, 2004). Furthermore, although BHTV detects fewer fractures than those observed in cores owing to its spatial resolution, BHTV is useful for determining the distribution of major fracture orientations (Genter et al., 1997).

The following protocols and definitions were used in this study: the determination of displacement using slickensteps (secondary fractures) and the classification of fault rocks are after the criteria of Petit (1987) and Sibson (1977), respectively. Also, faults with slip of less than 45° rake measured in the plane of the fault are defined as "predominantly strike-slip" faults, while, those faults at more than 45° rake, are "predominantly dip-slip" faults. No sense of slip direction of the hanging wall, either up dip or down, is implied. FCBs composed of fault planes with associated fault rocks such as breccia are defined as "major FCBs", whereas FCBs comprising fault planes with associated slickenlines and/or slickensteps (secondary fractures) but not fault rocks such as breccia are defined as "minor FCBs". FCBs include major FCBs and minor FCBs. Moreover, fractures with natural plumose structure are defined as "tensile fractures". Sample core photographs are shown in Fig. 5.

3.2. Mechanical characterization of host rock

Intact siliceous mudstone cores from the Wakkanai Formation were used for the rock mechanics studies. Tensile strength and internal friction angles for theoretical analyses using the Griffith–Coulomb criterion were obtained by Brazilian tests, after the Japanese industrial standards (JIS M 0303; Japanese Industrial Standard Committee, 2000), and triaxial compression tests after Kovari et al. (1983), respectively.

4. Results

Major FCBs, minor FCBs, tensile fractures, and bedding faults such as occur in the cleared, horizontal outcrop were intersected by the boreholes. The fault rocks associated with the major FCBs are mostly fault breccias (thickness: <30 cm), and seldom occur as fault gouge (thickness: <3 mm). The tensile fractures are outcrop-scale fractures which crosscut the bedding planes at high angles similar to those of the FCBs. Although splay cracks propagating from major FCBs were observed in the outcrop, they are classified as either tensile fractures or minor FCBs.

4.1. Fracture mapping of the horizontal outcrop

The strikes and sense of displacement along FCBs in the bedrock exposure are shown in Fig. 6a. The data on long, well linked faults were collected at many points along strike. The strikes of the FCBs are WNW–ESE, oblique to the direction of the fold axes, as is evident in Fig. 1 (i.e. N10°W). The sense of displacement is sinistral, predominantly strike-slip.

Crosscutting relationships between major FCBs and bedding faults show that the former always displace the latter (Fig. 7), generally with less than 0.6 m offset. Layered opaline chert is also present in this outcrop, but whether or not major FCBs displace the layered opaline chert is not clear because the layered opaline chert boundaries are so indistinct (Fig. 4) that with fault displacements of generally less than 0.6 m, any offset is difficult to recognize. Only the major FCBs in the center of the outcrop exhibit large enough

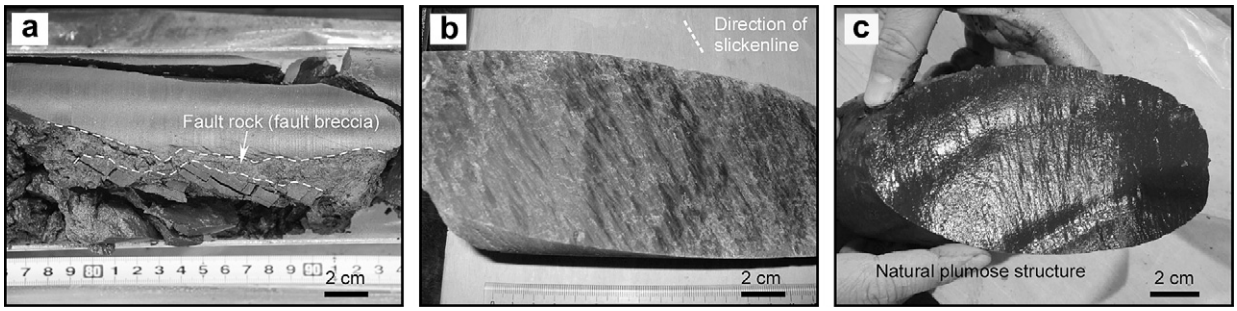

Fig. 5. Examples of fractures in core. (a) major FCB (370.8 m depth in HDB-6), (b) minor FCB (277.1 m depth in HDB-6), and (c) tensile fracture (377.1 m depth in PB-V01).

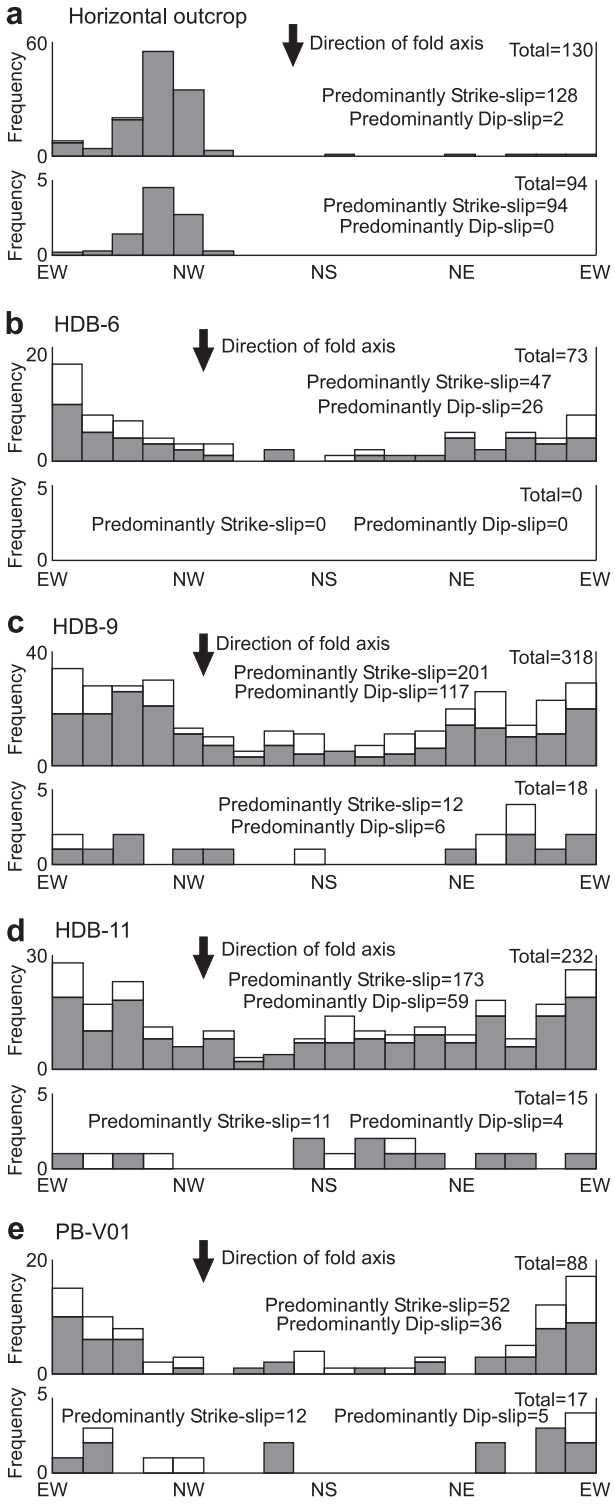

Fig. 6. Histograms showing the distribution of fault strikes and sense of displacement of FCBs. Upper and lower histograms in (a)–(e) show the data on major and minor FCBs and only on major FCBs, respectively. However, in the boreholes, only the data on the oriented faults determined by detailed correlation between core and BHTV imagery are shown. Gray and white bars indicate predominantly strike-slip and predominantly dip-slip, respectively.

offsets, (i.e. about 10 m) to determine that there has indeed been displacement of the layered opaline chert (Fig. 4).

In the outcrop, many splay cracks propagate from major FCBs. The splays are often in densely fractured zones at the major FCB tips

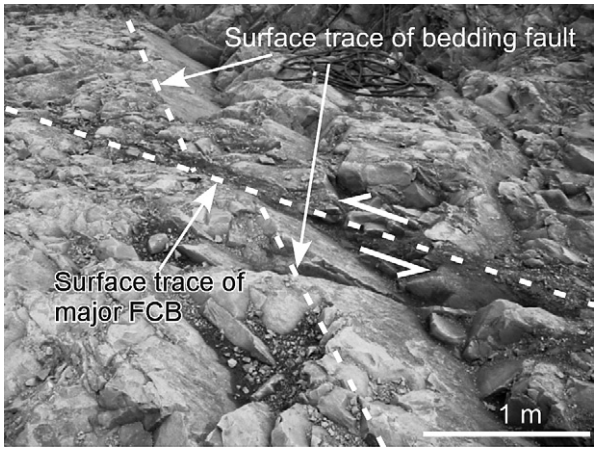

Fig. 7. Photograph showing the crosscutting relationship between a younger, major FCB and a bedding fault. Note the sinistral, predominantly strike-slip shear along the major FCB displacing the bedding fault with an offset of about 0.6 m.

or within the major FCB linkages, where the fault appears to have a left-step. The splay cracks strike 10–50° counterclockwise from the fault planes and have lengths of decimeters to meters, whereas the lengths of the linked fault segments are from meters to decameters (Figs. 8 and 9). Most splay cracks are tensile fractures and do not show any evidence of shearing although some splay cracks, particularly those within fault linkages, show evidence of shearing. These shear splay cracks are thought to be sheared tensile fractures which have originated as tensile fractures, because the orientation of the shear splay cracks is the same as those of the adjacent tensile splay cracks.

In addition, the major FCBs were shown to have slipped under a horizontal stress state with $\sigma 1$ normal to the fold axis and $\sigma 3$ parallel to the fold axis, determined by the multiple inverse method using the fault displacement data obtained at this outcrop (Ishii and Fukushima, 2006). Under this stress regime the above orientation of the evolving splay cracks is in agreement with those generally predicted by the numerical simulations of Lunn et al. (2008).

4.2. Fracture logging of the boreholes

Siliceous mudstones of the Wakkanai Formation were intersected by borehole HDB-6 from 262 m to 620 m depth; by HDB-9 from 0 m to 520 m depth; by HDB-11 from 460 m to 1020 m depth and by PB-V01 from 237 m to 520 m depth. Fractures in the core from these sections were examined. At shallower depths in boreholes HDB-6, HDB-11 and PB-V01, the diatomaceous mudstones of the Koetoi Formation were intersected. FCBs were commonly intersected by the boreholes; examination of recovered core indicated that for every 10 m long section of core there were between 0 and 44 FCBs with an average of 9.4 FCBs over 10 m long sections (frequency: 0–44 per 10 m, avg. 9.4 per 10 m). Additionally, 44% of the FCB population were oriented by detailed correlation between core and BHTV imagery. Moreover, 14% of the population of FCBs observed in core are major FCBs (frequency: 0–9 per 10 m, avg. 1.3 per 10 m), and 23% of the major FCB population could be oriented by detailed correlation with the BHTV imagery. Strikes of all the oriented FCBs are predominantly EW, oblique to the fold axes (i.e. N40°W: Fig. 1) though the FCBs with NNE–SWS-strikes, oblique to the fold axes as well as EW-strikes, are also recognized in HDB-11 (Fig. 6d), and the sense of displacement is predominantly strike-slip in each borehole (Fig. 6b–e). These observations are very similar to those on the FCBs in the horizontal outcrop. For those oriented major FCBs, their sense of displacement is predominantly strike-

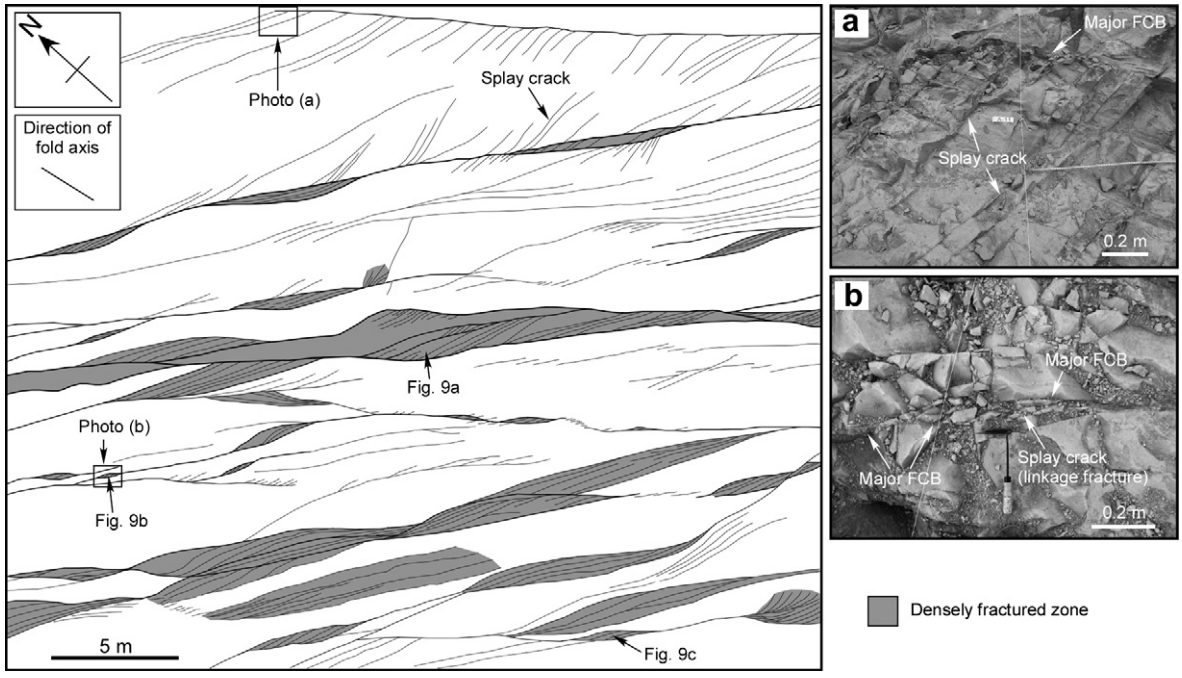

Fig. 8. (Left side) Sketch of fractures in the horizontal bedrock exposure except for bedding faults (modified from Ishii and Fukushima, 2006), (a) photograph of splay cracks propagating from a major FCB and (b) photograph of splay cracks (linkage fractures) within a major FCB linkage. In the left figure, thick lines represent major FCBs, while thin lines are minor FCBs and tensile fractures such as splay cracks. The sense of displacement of FCBs is sinistral, predominantly strike-slip. Note the left figure area corresponds to the clockwise at a right angle of Fig. 4.

slip (Fig. 6b–e), similar to the major FCBs in the outcrop. There is no systematic change in strike nor sense of displacement with depth.

In core from relatively great depths (e.g. below 400 m), en echelon shear fractures (minor FCBs) were sometimes observed to develop in extensions several centimeters long at and beyond the fault tips in directions parallel to the existing minor FCBs, although it should be remembered that the core diameter is only 86 mm. Thus at depth, shear fractures appear to propagate from fault tips in directions subparallel to the existing fault planes and parallel shear fractures form beyond the fault tips. Sense of displacement of those shear fractures is the same as for the existing minor FCBs. Examples are shown in Fig. 10. En echelon shear fractures occur more often at greater depths, e.g., in PB-V01, the average frequency is 1.0 per 100 m ($1\sigma = 1.4$) above 450 m, whereas, at greater depth, it is 6.0 per 100 m (one interval data). Similar trends are also observed in the other boreholes; 0.5 per 100 m ($1\sigma = 0.7$) above 400 m vs 1.5 per 100 m ($1\sigma = 0.7$) below 400 m in HDB-6; 1.0 per 100 m ($1\sigma = 1.7$) above 300 m vs 5.0 per 100 m ($1\sigma = 1.4$) below 300 m in HDB-9; and 2.0 per 100 m ($1\sigma = 1.9$) below 500 m in HDB-11. In addition, tensile fractures are also observed in core (frequency: 0–16 per 10 m, avg. 2.3 per 10 m, $1\sigma = 3.3$). Frequencies of the tensile fractures decrease with depth, e.g., in PB-V01, the average frequency is 3.3 per 10 m ($1\sigma = 3.6$) above 450 m, while, at greater depth, it is 1.6 per 10 m ($1\sigma = 2.7$). Similarities are found in the other boreholes; 3.2 per 10 m ($1\sigma = 4.0$) above 400 m vs 1.9 per 10 m ($1\sigma = 3.7$) below 400 m in HDB-6; 3.2 per 10 m ($1\sigma = 4.1$) above 300 m vs 2.0 per 10 m ($1\sigma = 2.3$) below 300 m in HDB-9; and 0.8 per 10 m ($1\sigma = 1.5$) below 500 m in HDB-11. Thus, en echelon shear fractures increase in number as depth increases, while tension fractures decrease in number.

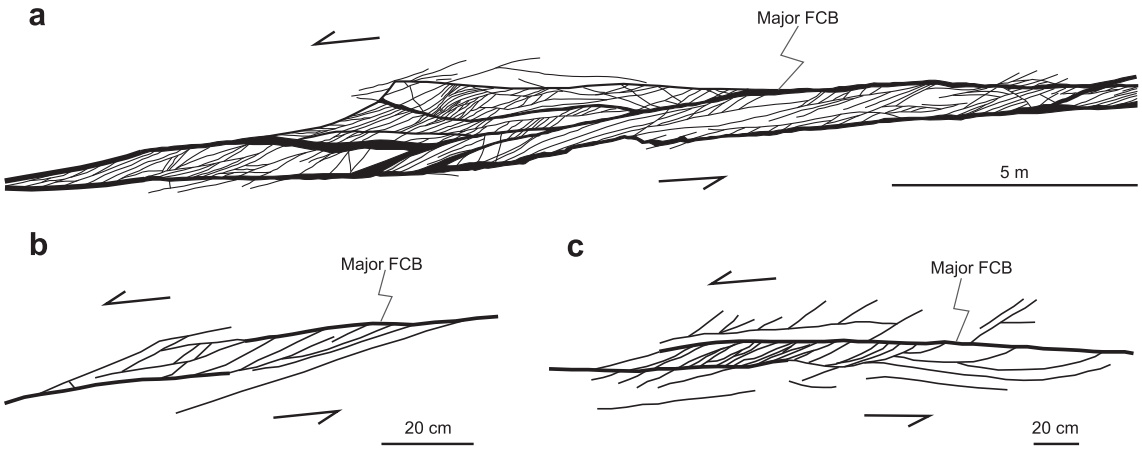

Fig. 9. Detailed sketches of the high density of fractures in the fault linkage zones shown in Fig. 8, where many splay cracks propagate from major FCBs (modified Ishii and Fukushima, 2006). Thick lines represent major FCBs and thin lines represent tensile fractures and minor FCBs. The splay cracks appear to have grown as internal tensile fractures, although some subsequently accommodated shear displacements. Eventually, their fractures form fault zones.

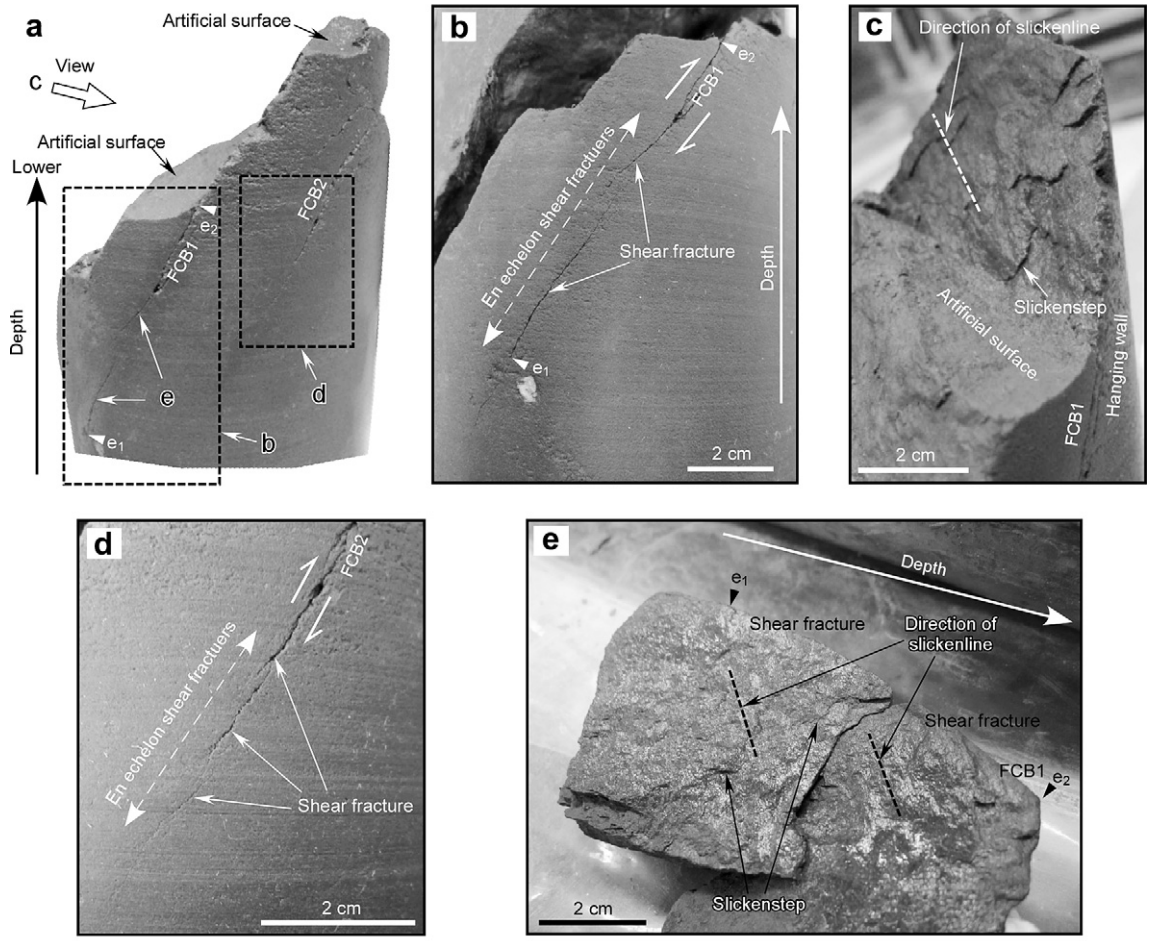

Fig. 10. En echelon shear fractures (minor FCBs) evolving at and beyond the minor FCB tips, FCB1 and FCB2 tips in this figure, at much lower angles to the existing fault planes (a core sample from 469.6 m depth in PB-V01). (a) an overview shot of the core sample (b) occurrence at and beyond the FCB1 tip, (c) hanging wall surface of the FCB1, (d) occurrence at and beyond the FCB2 tip, and (e) footwall surfaces of the shear fractures developing at and beyond the FCB1 tip. Splay fracturing was not observed near the FCB1 and FCB2 tips. Sense of displacement of the FCB1, FCB2 and shear fractures are the same; sinistral, predominantly strike-slip, although slickenlines and slickensteps of the shear fractures indicate only very weak shearing.

4.3. Rock mechanics tests: siliceous mudstone

Tensile strengths of 0.8 ± 0.1 MPa to 3.2 ± 0.3 MPa were obtained by Brazilian tests on siliceous mudstone core in 30–100 m intervals in each borehole. The average of the tensile strengths is 1.5 MPa ($1\sigma = 0.6$), though some tensile strengths exceeding 2 MPa were obtained (Fig. 11a). The core samples showing high tensile strength are from 303 m and 348 m depth in HDB-6 and from 272 m, 303 m and 402 m depth in PB-V01. These stratigraphic positions are in the upper part of the Wakkanai Formation. The fact that such harder siliceous mudstones are observed in the upper part of the Wakkanai Formation is consistent with the previous indication that additional silica cementation, which hardened siliceous mudstones, may often occur in the upper part of the opal-CT zone (near the opal-A zone) in Neogene noncalcareous siliceous rocks in northern Japan (Iijima and Tada, 1981).

Internal friction angles obtained by triaxial compression testing of cores from 300 m and 550 m depth in HDB-6 have values of $27.3 \pm 1.3°$ and $27.5 \pm 1.0°$ respectively, (avg. 27.4°), though tensile strengths on core from nearly the same depths are 3.1 ± 0.2 MPa and 0.9 ± 0.1 MPa respectively. Internal friction angles were also obtained from ten core samples of the Wakkanai Formation in the other boreholes (HDB-1 and HDB-2) (Niunoya and Matsui, 2005), and the average angle of internal friction for the twelve core samples from these boreholes (HDB-1, HDB-2 and HDB-6) is $26.1 \pm 2.9°$ (Fig. 11b).

5. Discussion

5.1. Relative age of formation of the major FCBs

The relative timing of fault formation can be inferred from their crosscutting relationships with other structures. The major FCBs displace bedding faults without exception. The bedding faults are considered to have formed synchronously with flexural folding (Ishii and Fukushima, 2006). Therefore, the later major FCBs are thought to have developed during and/or after uplift and erosion following folding. This deduction is also supported by observations from the horizontal outcrop where a major FCB displaces layered opaline chert, which is considered by Iijima and Tada (1981) to have formed during uplift and erosion. This implies the major FCBs were growing during and/or after uplift and erosion.

5.2. Stress state suitable for propagation of splay cracks in the Wakkanai Formation

What stress state would lead to the development of the abundant splay cracks that are seen to propagate from the major FCBs?

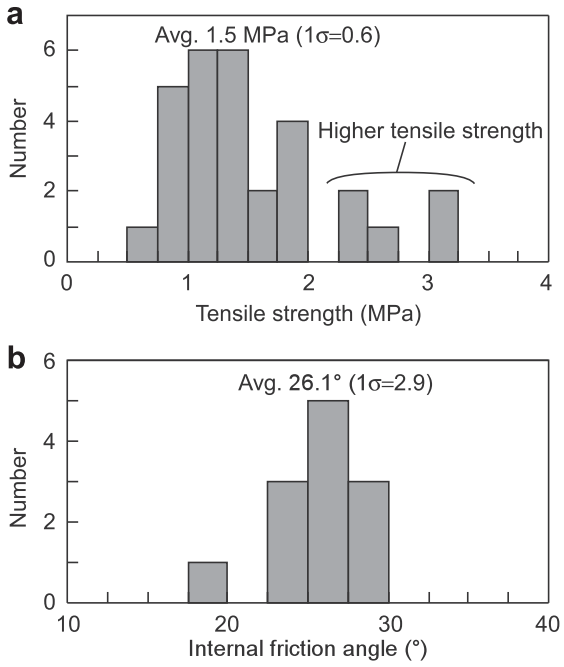

Fig. 11. Histograms on rock mechanical properties of the Wakkanai Formation measured by laboratory tests. (a) tensile strengths of core samples from HDB-6, HDB-9, HDB-11 and PB-V01 examined in this study. (b) internal friction angles of core samples from HDB-6 and boreholes HDB-1 and HDB-2 (Niunoya and Matsui, 2005).

Most splay cracks propagating from a fault can be formed as tensile fractures, particularly at the fault tips, by concentration of tensile stress generated when a slip patch nucleates and propagates in a fault (Martel and Pollard, 1989). But such tensile failure does not necessarily occur at the fault tips under all initial stress states. Previous numerical simulations suggest that shear failure can also occur at the fault tips following fault slip, resulting in propagation of shear fractures subparallel to the original fault plane or formation of shear fractures that propagated back into the compressive quadrants (Shen and Stephansson, 1993; Bourne and Willemse, 2001; Willson et al., 2007; Lunn et al., 2008). Although an extension of the initial fault in its own plane also has been previously simulated by Du and Aydin (1993, 1995), tensile failure is suppressed in their conceptual model of mechanical failure.

Following Bourne and Willemse (2001), the distance between any prevailing stress state in a rock mass to either the tensile or the shear failure conditions can be described by a stress quantity, X on a Mohr diagram. In Fig. 12, X corresponds to the shortest distance from the Griffith–Coulomb failure envelope of rock strength to the Mohr circle, the initial stress state. Brittle failure occurs when the Mohr circle stresses reach the failure envelope, i.e. $X = 0$, and the mode of failure is determined by whichever failure condition is met; either $X_{\mathrm{shear}}(X_s) = 0$ or $X_{\mathrm{tensile}}(X_t) = 0$. Furthermore, reduction of effective normal stress and increase of shear stress near fault tips, that are produced by fault slip (e.g., Martel and Pollard, 1989; Bourne and Willemse, 2001), are important factors causing brittle failure near fault tips.

When fault slip occurs under an initial stress state where X_s is smaller than X_t (Fig. 13a, top), two cases can be assumed for failure induced by reduction of effective normal stress and/or increase of shear stress near the fault tip (Fig. 13b). In the first case, shear failure occurs before tensile failure can occur (Fig. 13b, top), and, at least in the case of the Wakkanai Formation, en echelon shear fractures can develop at and beyond the fault tips in the plane of and thus parallel to the existing faults as shown in Fig. 10 and Fig. 13c, top. Shear fractures that propagate back into the

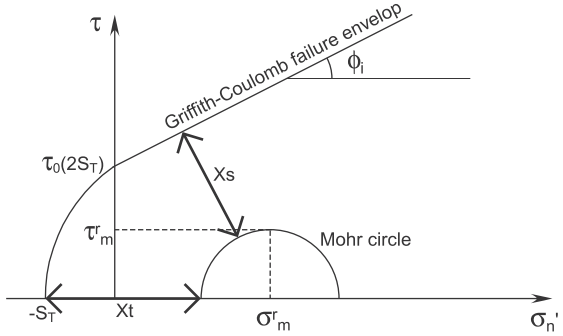

Fig. 12. Proximity of stress state to brittle failure conditions is represented by the smallest stress increment required to reach that stress state from either the shear failure envelope, X_s, or the tensile failure envelope, X_t: see Bourne and Willemse (2001); the cohesive strength, τ_0, is assumed to be equal to twice the tensile strength, S_T, following Brace (1960).

compressive quadrants were not observed in the outcrop. Eventually, the en echelon shear fractures would coalesce into a fault represented by fault rocks such as a major FCB. In the other case, tensile failure occurs before shear failure can occur (Fig. 13b, bottom) and splay cracks propagate from the fault tips by tensile failure (Fig. 13c, bottom).

However, when fault slip occurs in the initial stress state where X_s is larger than X_t (Fig. 13a, bottom), tensile failure will certainly occur before shear failure due to reduction of effective normal stress and increase of shear stress near the fault tip (Fig. 13b, bottom), and splay cracks will propagate from the fault tips by tensile failure. Therefore, the suitable stress state for propagation of the splay cracks in the Wakkanai Formation is likely to be the case where $X_s - X_t$ is positive, that is when $X_s > X_t$.

The above value of $X_s - X_t$ is written by the Griffith–Coulomb criterion as:

$$X_s - X_t = \frac{2S_T(\cos\phi_i - 0.5)}{(1 - \sin\phi_i)} - \sigma^r_m$$

where S_T, ϕ_i and σ^r_m are the tensile strength, the angle of internal friction, and the remote mean stress, respectively (Fig. 12). This formula means that failure modes which occur at fault tips by the fault slip depend on the tensile strength, the angle of internal friction, and the remote mean stress at the time of fault slip, and, in the case of rocks which do not significantly vary in both the tensile strength and the angle of internal friction, the lower remote mean stress is suitable for propagation of tensile splay cracks. This formula also means that higher values of the tensile strength promote tensile failure near fault tips when fault slip occurs while the lower values tend to induce shear failure, provided the remote mean stresses are similar (and the angles of internal friction are also). This can be consistent with the relationship between rock strengths and failure modes suggested by field observations of siliceous shale units of the Monterey Formation of coastal California (Gross, 1995; Dholakia et al., 1998; Eichhubl and Boles, 2000).

5.3. Estimation of $X_s - X_t$ distributions in the boreholes

In this study, the distributions of $X_s - X_t$ in the Wakkanai Formation in each borehole were estimated using the above formula, with tensile strengths and angles of internal friction determined by the laboratory testing and the assumed remote mean stresses. Tensile strengths were set as the strengths obtained by Brazilian tests (0.8–3.2 MPa) at depths in 50–100 m intervals in each borehole (Fig. 14). Although the internal friction angles

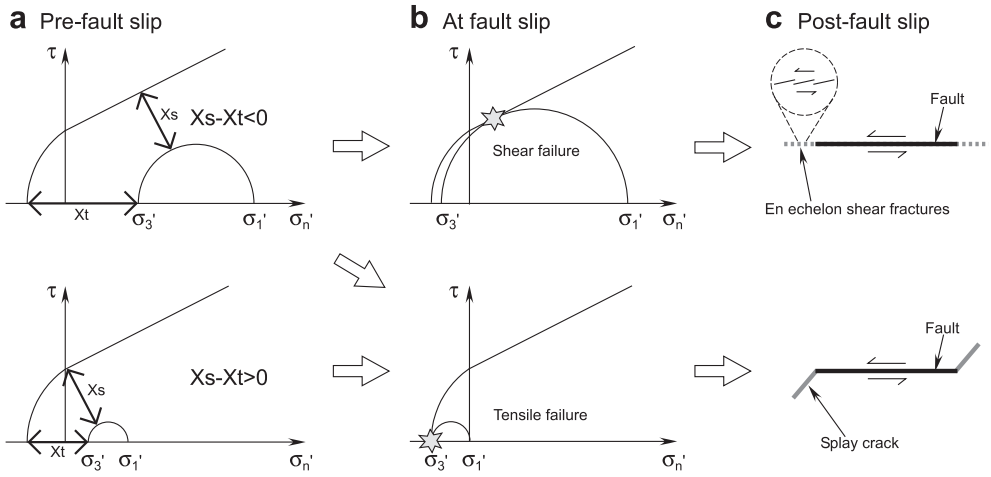

Fig. 13. Modes of brittle failure near the fault tip induced by reduction of effective normal stress and/or increase of shear stress that are produced by fault slip in the Wakkanai Formation. The failure modes are determined by the initial stress state. See Fig. 12 for the envelopes and circles.

obtained by the triaxial compression tests in the boreholes are only from two locations in HDB-6, the average angle of internal friction for the twelve core samples including core samples from the other boreholes (HDB-1 and HDB-2) is 26.1 ± 2.9° (Fig. 11b). In this study, considering variations in the internal friction angles, 20.3 and 31.9°, which are lower and higher than the average degree by 2σ (=5.8), were represented as the low angle case (Case 1) and the high angle case (Case 2) respectively (Fig. 14). For the remote mean stresses, the following was assumed: i) the principal remote stresses are horizontal and vertical based on the results of the multiple inverse

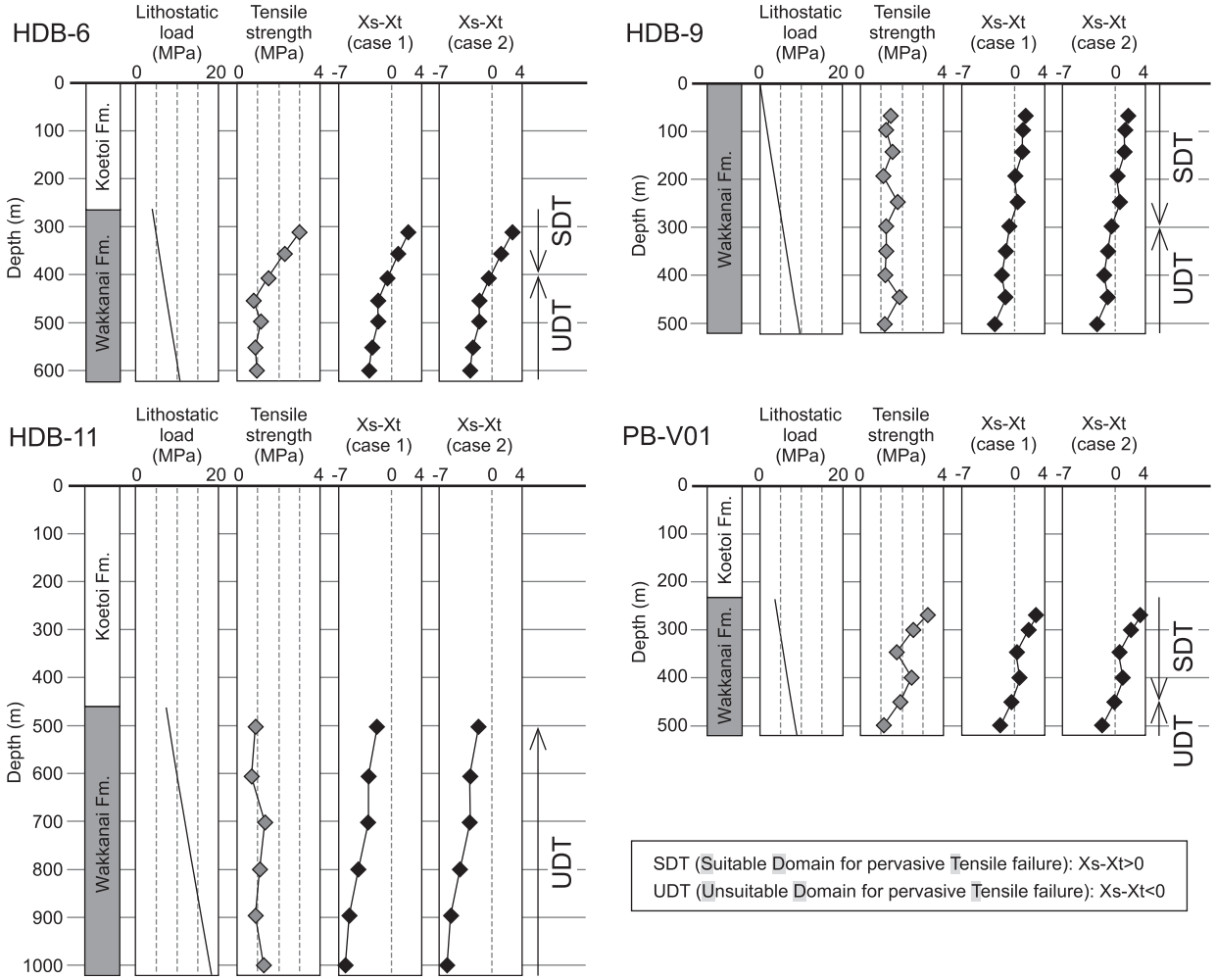

Fig. 14. The estimated depth profiles of $X_s - X_t$ estimated in each borehole. Results in Case 1 and Case 2 are based on a low friction angle (20.3°) and a high internal friction angle (31.9°) respectively, and the results are almost the same. The lithostatic load estimated by density logging and the tensile strengths determined by laboratory testing are also shown.

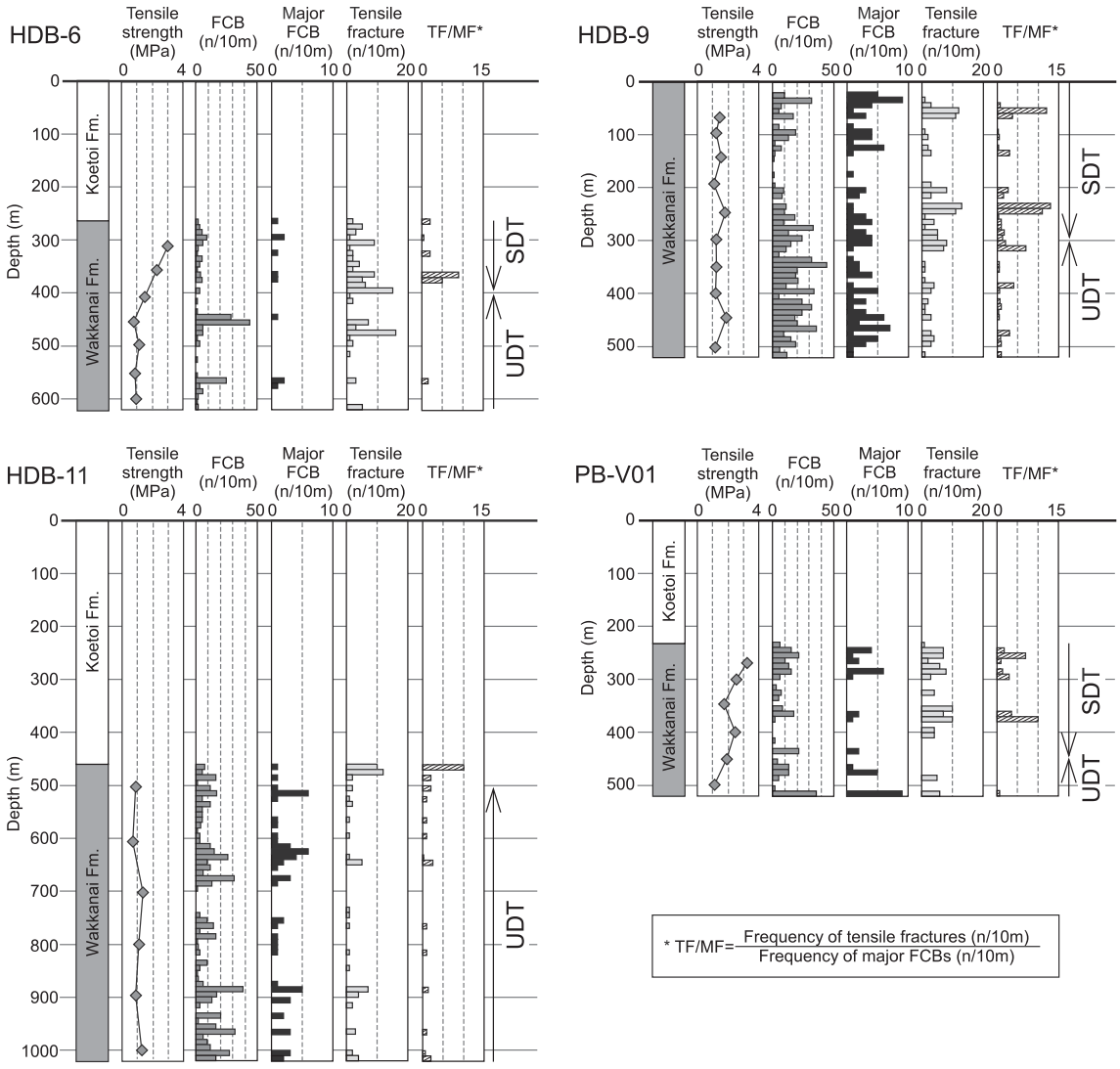

Fig. 15. Frequency distributions of brittle fractures in the boreholes in the Wakkanai Formation. Frequency is expressed as a number per 10 m for FCBs, major FCBs, and tensile fractures in each borehole. Also, tensile strengths, histograms showing the ratios of tensile fracture frequency to major FCB frequency, and the distribution of the SDT and UDT in each borehole are provided.

analyses using the fault slip data sampled in the horizontal outcrop, ii) the vertical stress is lithostatic, iii) the pore pressure is hydrostatic since the present pore pressures of the sections examined in the borehole are nearly under hydrostatic state (Kurikami, 2007; Funaki et al., 2009) and further the elevated pore pressure, which could have been raised during the early stage of folding following burial diagenesis (e.g., Engelder, 1985), are inferred to be nearly released by early fracturing predating the major FCBs development, and iv) the remote mean stress is a vertical effective stress as the sense of displacement of the major FCBs is predominantly strike-slip (Fig. 6). The lithostatic load was calculated using data obtained by density logging in each borehole (Fig. 14). Although the estimation based on the above assumptions is accompanied by some errors, the distribution of approximate $X_s - X_t$ could be determined.

The estimated depth profiles of $X_s - X_t$ in Case 1 and Case 2 are shown in Fig. 14. In this study, the domain where $X_s - X_t$ is positive is defined as SDT (Suitable Domain for pervasive Tensile failure), while, the domain where $X_s - X_t$ is negative is defined as UDT (Unsuitable Domain for pervasive Tensile failure). The results using upper and lower values for internal friction angle are almost the same (Fig. 14). The SDT domains are estimated to be above 400 m in HDB-6, above 300 m in HDB-9, and above 450 m in PB-V01, while the UDT domains were estimated to occur below these depths in HDB-6, in HDB-9, and in PB-V01, respectively and below 500 m in HDB-11 (the depth of the SDT domain in HDB-11 is unknown, but is no deeper than 500 m). Thus, the SDT and UDT domains roughly correspond to the rock mass above and below 400 m depth in each borehole, respectively, if we take into consideration estimation errors.

5.4. Comparison between the distribution of the SDT and UDT and fractures in core

The presence of many splay cracks along a fault is an indication of numerous slip events along a fault (Martel and Pollard, 1989). Similarly, a fault associated with fault rocks such as breccia is likely formed by several slip events. Hence, if tensile splay cracks are easily developed by fault slip in an SDT, the number of tensile fractures near major FCBs is expected to be higher in an SDT. Fig. 15 shows the frequencies (number per 10 m) of major FCBs and of tensile fractures, the ratios of the frequencies of tensile fractures to major FCBs, and the distributions, in terms of depth and boundaries, of the SDT and UDT in each borehole. Comparison of the ratios of tensile fracture to major FCB frequencies and the SDT/UDT

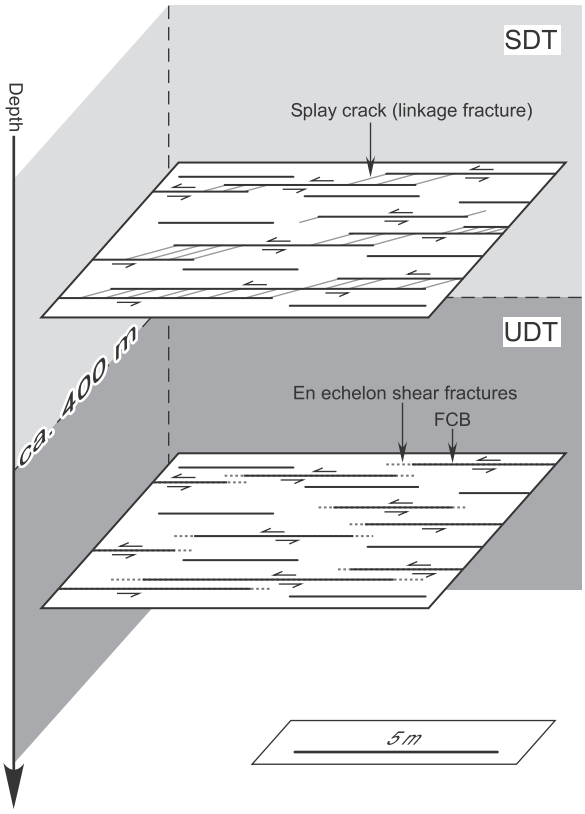

Fig. 16. A growth model of the major FCBs in the Wakkanai Formation during and/or after uplift and erosion. When fault slip occurs in an SDT domain, splay cracks form near the fault tips by tensile failure, resulting in faults strongly interconnected via numerous tensile splay cracks. In contrast, when fault slip is in a UDT domain, shear failure is predominant near fault tips and en echelon shear fractures could form at and beyond the fault tips.

distributions, indicate that the higher ratios (e.g. $\geq$5) are restricted, with one exception in HDB-9, to the SDT domain. The frequencies of tensile fractures also are higher in the SDT than the UDT. This evidence supports the above hypothesis. Although a considerable number of tensile fractures are observed also in the range of 470–480 m depth in HDB-6 in the UDT, it could be the result of the following: i) mechanical effects of slip on a considerable number of FCBs observed at 440–460 m depth (since tensile failure also can occur by fault slip even if within a UDT as shown in Fig. 13), or ii) error in estimation of the location of the SDT/UDT boundary (perhaps several tens meters) due to the assumptions relevant to the remote mean stresses at the time of fault slip.

Furthermore, the ratios of tensile fracture frequency to major FCB frequency are near zero throughout the defined UDT, though the frequency of major FCBs in the UDT (0–9 per 10 m; avg. 1.3 per 10 m) is similar to that in the SDT (0–9 per 10 m; avg. 1.4 per 10 m). This observation implies that the principal mode of failure in a UDT is shear. This implication is also supported by the fact that the occurrences of en echelon shear fractures developing at and beyond minor FCB tips in cores, i.e., those not associated with splays, were observed more often in the UDT than the SDT. This is based on both the frequency distribution of en echelon shear fractures mentioned in Section 4.2, and the SDT and UDT domains defined in Section 5.3.

Depths above 400 m in HDB-6 and the depths above 450 m in PB-V01 where tensile strengths are higher appear to correspond to the zones of high ratios of tensile fracture to major FCB frequencies and high frequencies of tensile fractures. But the zones with high ratios of tensile fracture to major FCB frequencies and high frequencies of tensile fractures are also recognized above 300 m depth in HDB-9, where tensile strengths are not higher. This shows that the failure mode near fault tips during faulting in the Wakkanai Formation, depends not only on rock strength, but also the remote mean stresses.

5.5. Growth model of the major FCBs

Concerning fault growth models in brittle sedimentary rocks, models in sandstones have been developed in previous studies. Two main ways that faults grow in sandstones are recognized (Davatzes et al., 2003; Flodin and Aydin, 2004): i) deformation band-based faulting; and ii) sheared-joint-based faulting. In the first model, faults grow by localization and amalgamation of individual deformation bands to form deformation band zones with subsequent coalescence of the zones and discontinuous slip surfaces nucleated along deformation bands to form through going deformation band-style faults (e.g. Aydin and Johnson, 1978; Antonellini and Aydin, 1995; Shipton and Cowie, 2001). In the second model, faults grow by linking with neighboring faults via linkage structures such as splay cracks, which formed near the fault tips by stress concentrations following slip nucleation on preexisting structures (e.g., Flodin and Aydin, 2004; Myers and Aydin, 2004). Although fault growth models in mudstones are seldom known, Dholakia et al. (1998) suggested that faults grew by linking via splay cracks produced by shearing along initial joints, i.e. the sheared-joint-based faulting model, in siliceous shale units of the Monterey Formation. In the case of the siliceous mudstone, the Wakkanai Formation, it is inferred by this study that, during and/or after uplift and erosion the major FCBs grew mainly by linking with adjacent faults via numerous splay cracks, which formed by tensile failure as shown in Figs. 8, 9 and Fig. 13c-bottom, in an SDT (i.e. above roughly 400 m depth). Such growth mechanism in an SDT domain is similar to the sheared-joint-based faulting model. In contrast, in a UDT (i.e. below roughly 400 m depth), the major FCBs grew predominantly by shear failure, and could develop in directions parallel to the fault planes through coalescence of the en echelon shear fractures as shown by Fig. 10, Fig. 13c, top and Fig. 16 though the developing direction would not necessarily be limited to the above directions. A fault growth model in mudstones like the mechanism in a UDT domain has not been reported, however, it may be similar to the idealized fault growth model suggested by Cowie and Scholz (1992).

5.6. Comparison between SDT and UDT and permeability of the Wakkanai Formation

Based on the above, the linking of adjacent, major FCBs via numerous tensile splay cracks is assumed to develop in an SDT. Previous studies pointed out that such structures associated with tensile fractures have important hydraulic properties. Eichhubl et al. (2009) showed by using the distribution of fault-related calcite cement at the Moab fault system in southern Utah as an indicator of paleofluid migration, that fluid flow was focused especially at locations of structural complexity such as fault intersections, extensional steps, and fault-segment terminations, where many tensile fractures developed. Dholakia et al. (1998) indicated that increased hydrocarbon concentrations in the Monterey Formation in the southern San Joaquin Valley and coastal California are almost exclusively associated with faults which grew through linkage via many tensile splay cracks. Khang et al. (2004) indicated by numerical simulations that geometry of the structures linking faults via tensile splay cracks plays an important role in fluid flow through the fracture network. Mazurek et al. (1998, 2003) and Lunn et al. (2008) also imply that linkage by structures such as tensile

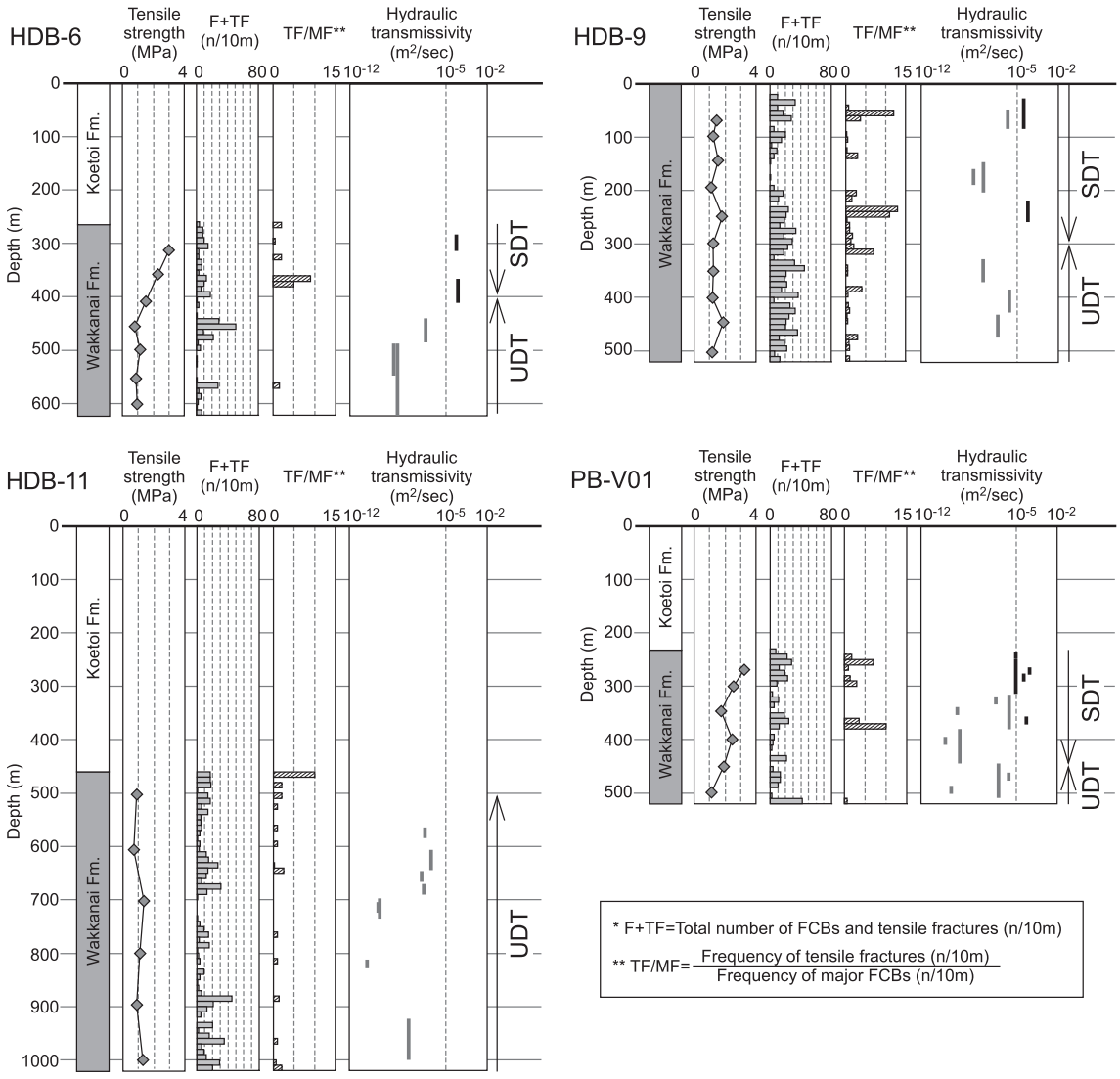

Fig. 17. Comparison of the SDT and UDT distributions and permeability in the Wakkanai Formation. Also, tensile strengths, the frequencies of total number of FCBs and tensile fractures and the ratios of tensile fracture frequency to major FCB frequency in each borehole are shown.

splay cracks may represent preferential pathways for fluid flow. In consideration of the work of these authors, comparisons between the distributions of SDT and UDT domains in each borehole and variations in permeability in the Wakkanai Formation were done in this study.

Fig. 17 shows the results of the comparisons in the each borehole. The SDT domains generally have higher permeability (e.g. hydraulic transmissivity: $\geq 10^{-5}$ m^2/s) whereas the UDT domains clearly show lower permeability (e.g. hydraulic transmissivity: $\leq 10^{-5}$ m^2/s). However, some lower permeability sections are also observed in the SDT domains in HDB-9 and PB-V01. These sections have relatively lower frequencies of total number of FCBs and tensile fractures and thus are not active in the main connected flow paths in an SDT. This observation suggests that the hydrogeological environment in an SDT differs from that in a UDT due to hydraulic effects of the faults strongly interconnected via many tensile splay cracks, and that these structures result in the restricted distribution of the highly permeable sections to depths less than about 400 m in the Wakkanai Formation, as shown in Figs. 3 and 17.

Diagenetic alteration products can also provide some indication of permeability of fractured rock masses (e.g., Milodowski et al., 1998; Solum et al., 2005; Eichhubl et al., 2009). But in the Wakkanai Formation, neither mineral precipitation on fractures nor alteration along fractures has been observed in core samples though oxidized zones along the major FCBs, which imply high permeability, are observed at surface (Ishii and Fukushima, 2006). Moreover, although the harder siliceous mudstones, which might be formed due to additional silica cementation during uplift as suggested by Iijima and Tada (1981), are observed in the subsurface, a relationship between the harder siliceous mudstones and permeability of the Wakkanai Formation has not been found. If the issue of whether or not some diagenetic indicator for fluid flow exists in the Wakkanai Formation is validated, further detailed X-ray analyses such as SEM, XRD and XRF must be done on rock matrices and fracture surfaces.

6. Conclusions

This paper discusses the growth mechanisms of the major FCBs in the Wakkanai Formation by the following methods: i) geological characterization by fracture mapping at an outcrop and by fracture logging in several boreholes; ii) rock mechanical characterization by laboratory tests on core samples for tensile strength and angle of

internal friction, and iii) theoretical analysis using the Griffith–Coulomb criterion. This paper suggests the following ideas:

1. The principal mode of failure, which occurs near fault tips by fault slip in the Wakkanai Formation, depends not only on rock strength, but also on the remote mean stresses.
2. During and/or after uplift and erosion the major FCBs grew mainly by linking with adjacent major FCBs via numerous splay cracks formed by tensile failure in an SDT (i.e. above roughly 400 m depth), while, in a UDT (i.e. below roughly 400 m depth), the major FCBs predominantly grow by shear failure, and could develop in directions parallel to the fault planes through coalescence of en echelon shear fractures though the direction of development is not necessarily limited to the above directions.
3. The hydrogeological environment in an SDT differs from that in a UDT due to hydraulic effects of the faults strongly interconnected via many tensile splay cracks. The preferential development of the linking structures results in the restricted distribution of the high permeability sections to less than about 400 m depth in the Wakkanai Formation.

Such conclusions are useful also for three dimensional geological modeling and for groundwater flow simulations (e.g., for the geological disposal of high level radioactive waste). However, in order to conduct the more detailed modeling and simulations for the Wakkanai Formation, it may be necessary to solve unanswered questions, such as the comprehensive deformation history, and the detailed hydraulic effects of the faults strongly interconnected via many tensile splay cracks.

Acknowledgements

We thank G. McCrank and W.R. Alexander for English editing and their helpful suggestions on this manuscript. We also express our gratitude to H. Moir, J.G. Solum and Z. Shipton for their critical review of the manuscript.

Appendix

The acronyms and their definition used in this study are as shown in Table A1.

Table A1
Acronyms and definitions.

Acronym	Definition
FCB	Fault crosscutting bedding planes at a high angle
Major FCB	FCB composed of fault planes with associated fault rocks such as breccia
Minor FCB	FCB composed of fault planes with associated slickenlines and/or slickensteps but not fault rocks such as breccia
X	Shortest distance from the Griffith–Coulomb failure envelope of rock strength to the Mohr circle
X_s	Shortest distance from the Coulomb failure envelope of rock strength to the Mohr circle
X_t	Shortest distance from the Griffith failure envelope of rock strength to the Mohr circle
SDT	Suitable domain for pervasive tensile failure
UDT	Unsuitable domain for pervasive tensile failure

References

Andersson, J., Ahokas, H., Hudson, J.A., Koskinen, L., Luukkonen, A., Löfman, J., Keto, V., Pitkänen, P., Mattila, J., Ikonen, A.T.K., Ylä-Mella, M., 2007. Olkiluoto Site Description 2006. POSIVA Technical Report POSIVA 2007-03, Olkiluoto, Finland.

Antonellini, M., Aydin, A., 1995. Effect of faulting on fluid flow in porous sandstone: geometry and spatial distribution. American Association of Petroleum Geologist Bulletin 79, 642–671.

Aydin, A., Johnson, A.M., 1978. Development of faults as zones of deformation bands and as slip surfaces in sandstone. Pure and Applied Geophysics 116, 931–942.

Bossart, P., Hermanson, J., Mazurek, M., 2001. Analysis of fracture network based on the integration of structural and hydrogeological observations on different scales. SKB Technical Report 01-21, SKB, Stockholm, Sweden.

Bourne, S.J., Willemse, E.J.M., 2001. Elastic stress control on the pattern of tensile fracturing around a small fault network at Nash Point, UK. Journal of Structural Geology 23, 1753–1770.

Brace, W.F., 1960. An extension of the Griffith theory of fracture to rocks. Journal of Geophysical Research 65, 3477–3480.

Caine, J.S., Evans, J.P., Forster, C.B., 1996. Fault zone architecture and permeability structure. Geology 24, 1025–1028.

Cowie, P.A., Scholz, C.H., 1992. Physical explanation for displacement-length relationship of faults using a post-yield fracture mechanics model. Journal of Structural Geology 14, 1133–1148.

d'Alessio, M.A., Martel, S.J., 2004. Fault terminations and barriers to fault growth. Journal of Structural Geology 26, 1885–1896.

Davatzes, N.C., Aydin, A., Eichhubl, P., 2003. Overprinting faulting mechanisms during the development of multiple fault sets, Chimney Rock fault array, Utah, USA. Tectonophysics 363, 1–18.

Dholakia, S.K., Aydin, A., Pollard, D.D., Zoback, M.D., 1998. Fault-controlled hydrocarbon pathways in the Monterey Formation, California. American Association of Petroleum Geologist Bulletin 82, 1551–1574.

Du, Y., Aydin, A., 1993. The maximum distortional strain energy density criterion for shear fracture propagation with applications to the growth paths of en échelon faults. Geophysical Research Letters 20, 1091–1094.

Du, Y., Aydin, A., 1995. Shear fracture patterns and connectivity at geometric complexities along strike-slip faults. Journal of Geophysical Research 100, 18093–18102.

Eichhubl, P., Boles, J.R., 2000. Focused fluid flow along faults in the Monterey Formation, coastal California. Geological Society of America Bulletin 112, 1667–1679.

Eichhubl, P., Davatzes, N.C., Becker, S.P., 2009. Structural and diagenetic control of fluid migration and cementation along the Moab fault, Utah. American Association of Petroleum Geologist Bulletin 93, 653–681.

Engelder, T., 1985. Loading paths to joint propagation during a tectonic cycle: an example from the Appalachian Plateau, U.S.A. Journal of Structural Geology 7, 459–476.

Evans, J.P., Forster, C.B., Goddard, J.V., 1997. Permeability of fault-related rocks, and implications for hydraulic structure of fault zones. Journal of Structural Geology 19, 1393–1404.

Flodin, E.A., Aydin, A., 2004. Evolution of a strike-slip fault network, Valley of Fire State Park, southern Nevada. Geological Society of America Bulletin 116 (1/2), 42–59.

Fukusawa, H., 1985. Late Neogene Formations in the Tempoku-Haboro region, Hokkaido, Japan – stratigraphic reinvestigation of the "Wakkanai" and "Koetoi" Formations. The Journal of the Geological Society of Japan 91, 833–849.

Funaki, H., Ishii, E., Tokiwa, T., 2009. Evaluation of the role of fracture as the major water-conducting feature in Neogene sedimentary rocks. Journal of the Japan Society of Engineering Geology 50, 239–248.

Genter, A., Castaing, C., Dezayes, C., Tenzer, H., Traineau, H., Villemin, T., 1997. Comparative analysis of direct (core) and indirect (borehole imaging tools) collection of fracture data in the Hot Dry Rock Soultz reservoir (France). Journal of Geophysical Research 102, 15419–15431.

Gross, M.R., 1995. Fracture partitioning: failure mode as a function of lithology in the Monterey Formation of coastal California. Geological Society of America Bulletin 107, 779–792.

Gutmanis, J.C., Lanyon, G.W., Wynn, T.J., Watson, C.R., 1998. Fluid flow in faults: a study of fault hydrogeology in Triassic sandstone and Ordovician volcaniclastic rocks at Sellafield, north-west England. Proceedings of the Yorkshire Geological Society 52, 159–175.

Hiraga, N., Ishii, E., 2008. Mineral and Chemical Composition of Rock Core and Surface Gas Composition in Horonobe Underground Research Laboratory Project (Phase 1). JAEA Technical Report JAEA-Data/Code 2007-022. Japan Atomic Energy Agency, Tokai-mura, Japan.

Iijima, A., Tada, R., 1981. Silica diagenesis of Neogene diatomaceous and volcaniclastic sediments in northern Japan. Sedimentology 28, 185–200.

Ikeda, Y., 2002. The origin and mechanism of active folding in Japan. Active Fault Research 22, 67–70.

Isaacs, C.M., 1982. Influence of rock composition on kinematics of silica phase changes in the Monterey Formation, Santa Barbara area, California. Geology 10, 304–308.

Ishii, E., Fukushima, T., 2006. A case study of analysis of faults in Neogene siliceous rocks. Journal of the Japan Society of Engineering Geology 47, 280–291.

Ishii, E., Yasue, K., Tanaka, T., Tsukuwi, R., Matsuo, K., Sugiyama, K., Matsuo, S., 2006. Three-dimensional distribution and hydrogeological properties of the Omagar Fault in the Horonobe area, northern Hokkaido, Japan. The Journal of the Geological Society of Japan 112, 301–314.

Ishii, E., Hama, K., Kunimaru, T., Sato, H., 2007. Change in groundwater pH by infiltration of meteoric water into shallow part of marine deposits. The Journal of the Geological Society of Japan 113, 41–52.

Ishii, E., Yasue, K., Ohira, H., Furusawa, A., Hasegawa, T., Nakagawa, M., 2008. Inception of anticline growth near the Omagari Fault, northern Hokkaido, Japan. The Journal of the Geological Society of Japan 114, 286–299.

Japanese Industrial Standard Committee, 2000. Method of Test for Tensile Strength of Rock JIS M 0303. Japanese Standards Association, Tokyo, Japan.
Khang, N.D., Watanabe, K., Saegusa, H., 2004. Fracture step structure: geometrical characterization and effects on fluid flow and breakthrough curve. Engineering Geology 75, 107–127.
Kovari, K., Tisa, A., Einstein, H.H., Franklin, J.A., 1983. Suggested methods for determining the strength of rock materials in triaxial compression: revised version. International Journal of Rock Mechanics and Mining Sciences 20, 283–290.
Kulander, B.R., Dean, S.L., Ward Jr., B.J., 1990. Fractured core analysis: interpretation, logging, and use of natural and induced fractures in core. In: AAPG Methods in Exploration Series 8. AAPG, Oklahoma, USA.
Kurikami, H., 2007. Groundwater Flow Analysis in the Horonobe Underground Research Laboratory Project: Recalculation based on the Investigation until Fiscal Year 2005. JAEA Technical Report JAEA-Research 2007-036. Japan Atomic Energy Agency, Tokai-mura, Japan.
Kurikami, H., Takeuchi, R., Yabuuchi, S., 2008. Scale effect and heterogeneity of hydraulic conductivity of sedimentary rocks at Horonobe URL site. Physics and Chemistry of the Earth Parts A/B/C 33 (Suppl. 1), S37–S44.
Lunn, R.J., Willson, J.P., Shipton, Z.K., Moir, H., 2008. Simulating brittle fault growth from linkage of preexisting structures. Journal of Geophysical Research 113, B07403. doi:10.1029/2007JB005388.
Martel, S.J., Pollard, D.D., 1989. Mechanics of slip and fracture along small faults and simple strike-slip fault zones in granitic rock. Journal of Geophysical Research 94, 9417–9428.
Mazurek, M., 1998. Geology of the crystalline basement of northern Switzerland and derivation of geological input data for safety assessment models. NAGRA Technical Report NTB 93-12, NAGRA, Wettingen, Switzerland.
Mazurek, M., 2000. Geological and hydraulic properties of water-conducting features in crystalline rocks. In: Stober, I., Bucher, K. (Eds.), Hydrogeology of Crystalline Rocks. Kluwer Academic Publishers, Dordrecht, Netherlands, pp. 3–26.
Mazurek, M., Bossart, P., Eliasson, T., 1996. Classification and characterization of water-conducting features at Äspö: results of investigations on the outcrop scale. SKB International Cooperation Report ICR 97-01, SKB, Stockholm, Sweden.
Mazurek, M., Lanyon, G.W., Vomvoris, S., Gautschi, A., 1998. Derivation and application of a geologic dataset for flow modeling by discrete fracture networks in low-permeability argillaceous rocks. Journal of Contaminant Hydrology 35, 1–17.
Mazurek, M., Jakob, A., Bossart, P., 2003. Solute transport in crystalline rocks at Äspö – I: geological basis and model calibration. Journal of Contaminant Hydrology 61, 157–174.
Milodowski, A.E., Gillespie, M.R., Naden, J., Fortey, N.J., Shepherd, T.J., Pearce, J.M., Metcalfe, R., 1998. The petrology and paragenesis of fracture mineralisation in the Sellafield area, west Cumbria. Proceedings of the Yorkshire Geological Society 52, 215–241.
Mitsui, K., Taguchi, K., 1977. Silica mineral diagenesis in Neogene tertiary shales in the Tempoku district, Hokkaido, Japan. Journal of Sedimentary Petrology 47, 158–167.
Murata, K.J., Nakata, J.K., 1974. Cristobalitic stage in the diagenesis of diatomaceous shale. Science 184, 567–568.
Myers, R., Aydin, A., 2004. The evolution of faults formed by shearing across joint zones in sandstone. Journal of Structural Geology 26, 947–966.
Niunoya, S., Matsui, H., 2005. The Investigation on Rock Mechanics in HDB-1 and HDB-2 Boreholes in order to Select the URL Area. JNC Technical Report TN5400 2005-012. Japan Nuclear Cycle Development Institute, Tokai-mura, Japan.
Nordqvist, R., Gustafsson, E., Andersson, P., Thur, P., 2008. Groundwater flow and hydraulic gradients in fractures and fracture zones at Forsmark and Oskarshamn. SKB Technical Report R-08-103, SKB, Stockholm, Sweden.
Öhman, J., Niemi, A., Tsang, C.-F., 2005. Probabilistic estimation of fracture transmissivity from Wellbore hydraulic data accounting for depth-dependent anisotropic rock stress. International Journal of Rock Mechanics and Mining Sciences 42, 793–804.
Ota, K., Abe, H., Yamaguchi, T., Kunimaru, T., Ishii, E., Kurikami, H., Tomura, G., Shibano, K., Hama, K., Matsui, H., Niizato, T., Takahashi, K., Niunoya, S., Ohara, H., Asamori, K., Morioka, H., Funaki, H., Shigeta, N., Fukushima, T., 2007. Horonoe Underground Research Laboratory Project, synthesis of Phase I investigations 2001–2005. JAEA Technical Report JAEA-Research 2007-044. Japan Atomic Energy Agency, Tokai-mura, Japan.
Petit, J.P., 1987. Criteria for the sense of movement on fault surfaces in brittle rocks. Journal of Structural Geology 9, 597–608.
Rhén, I., Forsmark, T., Forssman, I., Zetterlund, M., 2006. Evaluation of hydrogeological properties for Hydraulic Conductor Domain (HCD) and Hydraulic Rock Domains (HRD). SKB Technical Report R-06-22, SKB, Stockholm, Sweden.
Segall, P., Pollard, D.D., 1983. Nucleation and growth of strike slip faults in granite. Journal of Geophysical Research 88, 555–568.
Shen, B., Stephansson, O., 1993. Numerical analysis of mixed Mode I and Mode II fracture propagation. International Journal of Rock Mechanics and Mining Sciences 30, 861–867.
Sibson, R.H., 1977. Fault rocks and fault mechanisms. Journal of Geological Society 133, 191–213.
Shipton, Z.K., Cowie, P.A., 2001. Damage zone and slip-surface evolution over μm to km scales in high-porosity Navajo sandstone, Utah. Journal of Structural Geology 23, 1825–1844.
Solum, J.G., van der Pluijim, B.A., Peacor, D.R., 2005. Neocrystallization, fabrics and age of clay minerals from an exposure of the Moab Fault, Utah. Journal of Structural Geology 27, 1563–1576.
Tada, R., Iijima, A., 1982. Petrology and diagenetic changes of Neogene siliceous rocks in northern Japan. Journal of Sedimentary Petrology 53, 911–930.
Twiss, R.J., Moores, E.M., 2007. Structural Geology, second ed. W.H. Freeman and Company, New York.
Wei, D., Seno, T., 1998. Determination of the Amurian plate motion. In: Flower, M., Chung, S.L., Lo, C.H., Lee, T.Y. (Eds.), Mantle Dynamics and Plate Interactions in East Asia. Geodynamics Series 27. American Geophysical Union, Washington, D.C., USA, pp. 337–346.
Wei, Z.Q., Egger, P., Descoeudres, F., 1995. Permeability predictions for jointed rock masses. International Journal of Rock Mechanics and Mining Sciences 32, 251–261.
Welch, M.J., Davies, R.K., Knipe, R.J., 2009. A dynamic model for fault nucleation and propagation in a mechanically layered section. Tectonophysics. doi:10.1016/j.tecto.2009.04.025.
Williams, J.H., Johnson, C.D., 2004. Acoustic and optical borehole-wall imaging for fractured-rock aquifer studies. Journal of Applied Geophysics 55, 151–159.
Willson, J.P., Lunn, R.J., Shipton, Z.K., 2007. Simulating spatial and temporal evolution of multiple wing cracks around faults in crystalline basement rocks. Journal of Geophysical Research 112, B08408. doi:10.1029/2006JB004815.
Yabuuchi, S., Kunimaru, T., Ishii, E., Hatsuyama, Y., Ijiri, Y., Matsuoka, K., Ibara, T., Matsunami, S., Makino, A., 2008. Horonobe Underground Research Laboratory Project, Overview of the Pilot Borehole Investigation of the Ventilation Shaft (PB-V01): Hydrogeological Investigation. JAEA Technical Report JAEA-Data/Code 2008-026. Japan Atomic Energy Agency, Tokai-mura, Japan.
Yamaji, A., 2000. The multiple inverse method: a new technique to separate stresses from heterogeneous fault-slip data. Journal of Structural Geology 22, 441–452.
Yamamoto, H., 1979. The geologic structure and the sedimentary basin off northern part of the Hokkaido Island. Journal of the Japanese Association of Petroleum Technologists 44, 260–267.